JEM Journal of Experimental Medicine

BRIEF DEFINITIVE REPORT

Spatial distribution and function of T follicular regulatory cells in human lymph nodes

Ismail Sayin[1,2,3*], Andrea J. Radtke[4*], Laura A. Vella[5], Wenjie Jin[1,2], E. John Wherry[5], Marcus Buggert[6], Michael R. Betts[5], Ramin S. Herati[5,7], Ronald N. Germain[4], and David H. Canaday[1,2]

T follicular regulatory (Tfr) cells are a population of CD4$^+$ T cells that express regulatory T cell markers and have been shown to suppress humoral immunity. However, the precise mechanisms and location of Tfr-mediated suppression in the lymph node (LN) microenvironment are unknown. Using highly multiplexed quantitative imaging and functional assays, we examined the spatial distribution, suppressive function, and preferred interacting partners of Tfr cells in human mesenteric LNs. We find that the majority of Tfr cells express low levels of PD-1 and reside at the border between the T cell zone and B cell follicle, with very few found in the germinal centers (GCs). Although PD-1$^+$ Tfr cells expressed higher levels of CD38, CTLA-4, and GARP than PD-1^{Neg} Tfr cells, both potently suppressed antibody production in vitro. These findings highlight the phenotypic diversity of human Tfr cells and suggest that Tfr-mediated suppression is most efficient at the T-B border and within the follicle, not in the GC.

Introduction

Humoral immunity is dependent on T follicular helper (Tfh) cells, a subset of CD4$^+$ T cells that reside in the follicle and provide help to B cells via the secretion of cytokines such as IL-4 and IL-21 and expression of costimulatory molecules, especially CD40L (Crotty, 2014). In addition to Tfh cells, a subset of CD4$^+$ regulatory T cells (Treg cells) termed follicular regulatory T (Tfr) cells has been found in the lymphoid organs and blood of animals and humans (Chung et al., 2011; Linterman et al., 2011; Wollenberg et al., 2011; Vaeth et al., 2014; Wallin et al., 2014; Chowdhury et al., 2015). Although first identified in human tonsils (Lim et al., 2004), much of the biology and function of Tfr cells has been elucidated in mouse models (Chung et al., 2011; Linterman et al., 2011; Wollenberg et al., 2011; Sage et al., 2013, 2014; Sage and Sharpe, 2015). These studies revealed that Tfr cells originate from thymic-derived Treg cells and share the following characteristics with Tfh and Treg cells: expression of the transcription factors BCL6, FOXP3, and BLIMP-1, the IL-2 receptor α chain CD25, the inhibitory receptor CTLA-4, the chemokine receptor CXCR5, costimulator ICOS, and coinhibitor PD-1.

Although there is strong evidence that Tfr cells can suppress Tfh and B cells (Chung et al., 2011; Linterman et al., 2011; Wollenberg et al., 2011; Wallin et al., 2014; Chowdhury et al., 2015; Miles et al., 2015; Sage and Sharpe, 2015), how, where within lymphoid tissues, and on what cell populations Tfr cells exert their regulatory functions remain uncertain. Addressing mechanistic issues of human immune cell function that play out within complex tissue environments is difficult, and most functional studies are conducted solely using cells isolated from their natural tissue environment. Here we have combined such in vitro functional studies with quantitative, multiplexed immunohistochemistry (histo-cytometry; Gerner et al., 2012) to provide insight into the spatial distribution, interacting partners, and function of Tfr cells in human LNs. Together, our data suggest a model for Tfr cell activity in which their suppressive function is primarily mediated outside of the germinal center (GC).

Results and discussion

Quantitative imaging of Tfr cells in human mesenteric LNs (mLNs)

Previous studies have visualized the presence of FOXP3-expressing T cells in the follicles and GCs of human and mouse LNs using two- to four-color immunofluorescence and/or immunohistochemistry (Lim et al., 2004, 2005; Chung et al., 2011; Linterman

[1]Division of Infectious Diseases and HIV Medicine, Case Western Reserve University, Cleveland, OH; [2]Cleveland Veterans Affairs Geriatric Research Education and Clinical Center, Cleveland, OH; [3]Department of Biology, Case Western Reserve University, Cleveland, OH; [4]Lymphocyte Biology Section, Laboratory of Immune System Biology, National Institute of Allergy and Infectious Diseases, National Institutes of Health, Bethesda, MD; [5]Institute for Immunology and Department of Microbiology, University of Pennsylvania Perelman School of Medicine, Philadelphia, PA; [6]Center for Infectious Medicine, Department of Medicine, Karolinska Institutet, Stockholm, Sweden; [7]Department of Medicine, University of Pennsylvania, Philadelphia, PA.

*I. Sayin and A.J. Radtke contributed equally to this paper; Correspondence to David H. Canaday: dxc44@case.edu; Andrea J. Radtke: andrea.radtke@nih.gov.

et al., 2011; Wollenberg et al., 2011; Sage et al., 2013; Miles et al., 2015). Although a few of these studies assessed the number and location of FOXP3$^+$ T cells (Lim et al., 2005; Miles et al., 2015), no study has determined whether Tfr cells directly interact with Tfh cells in the GC or B cell follicle. To address this, we examined histological sections from human mLNs with a DNA marker (JOJO-1) and antibodies specific for BCL6, CD3, CD20, CD25, FOXP3, and PD-1 (Fig. 1 A). Because of panel design constraints, we were unable to simultaneously examine CD3, CD4, and CD25; however, 94% of CD3$^+$FOXP3$^+$ Tfr cells were CD4$^+$ (Fig. S1, A and B). The resulting images were analyzed by histo-cytometry, a quantitative imaging technique able to provide detailed information on the phenotype and distribution of cells in situ (Gerner et al., 2012; Fig. 1 B). PD-1 was abundantly expressed on Tfh cells (CD3$^+$FOXP3$^-$CD25$^-$ T cells), but was undetectable and/or low on all but a small fraction of Tfr cells (CD3$^+$FOXP3$^+$CD25$^+$) residing in the B cell follicle (CD20$^+$ region) and GC (BCL6$^+$ region) of the LNs (Fig. 1 A). Additionally, BCL6 was rarely detected in Tfr cells and found in a minority of Tfh cells analyzed by confocal microscopy, histo-cytometry, and flow cytometry (Fig. 1, A–C; and Fig. S1 C). These observations are consistent with the likelihood that human Tfh and Tfr cells down-regulate BCL6 protein after antigen exposure as previously reported for mouse Tfh cells (Kitano et al., 2011). Based on our imaging observations in which anatomical location is critical to calling a cell "follicular," we defined Tfr cells as CD3$^+$FOXP3$^+$CD25$^+$ cells and Tfh cells as CD3$^+$PD-1$^+$FOXP3$^-$CD25$^-$ (Fig. 1 B). Although CD25^{Neg} Tfr cells were recently identified in mice and humans (Ritvo et al., 2017; Wing et al., 2017), we found that >93% of CD3$^+$FOXP3$^+$ T cells present in the B cell follicles and GCs of human mLNs were CD25$^+$ based on confocal imaging (Fig. S1 D). Using flow cytometry, we confirmed that Tfr cells express higher levels of CD25 as compared with naive CD4$^+$ T cells and Tfh cells (Fig. S1 E).

Because histo-cytometry additionally preserves positional data, we quantified the number of Tfh and Tfr cells by "spatial gating" using the following anatomical regions: B cell follicle (defined by CD20$^+$ cells), GC (defined by BCL6$^+$ cells) and T-B border (within 50 µm of the CD20$^+$-defined B cell follicle; Fig. 1 B). Tfh cells outnumbered Tfr cells in all regions examined with a median Tfh/Tfr ratio of 1.3:1, 2:1, and 24:1 in the T-B border, B cell follicle, and GC, respectively (Fig. 1 D). Based on previous studies, and our in vitro data (see below) showing that these ratios are directly correlated with the capacity of Tfr cells to control humoral immunity, these findings imply that Tfr cells exert their regulatory functions outside of the GC. This conclusion is supported by the actual number of Tfr cells in the different regions of the LN; the majority of Tfr cells were found at the T-B border and not in the GC (mean = 8; Fig. 1 D). This finding was observed across multiple subjects and, although not emphasized in previous studies, is consistent with the images in prior publications (Lim et al., 2005; Chung et al., 2011; Linterman et al., 2011; Sage et al., 2013).

To gain insight into the cellular processes that might be regulated by Tfr cells close to or, for the few cells found there, within the GC, we examined their distribution within the light zone (LZ) and dark zone (DZ). Because follicular dendritic cells formed extensive networks throughout the follicle and could not be used to define the LZ in human mLNs (Fig. S1 A), we used the enrichment of Tfh cells and high expression of the cell proliferation marker Ki-67 to demarcate the LZ and DZ, respectively. We observed a higher proportion of GC Tfr cells in the LZ (Fig. S1 F); however, the density of Tfr cells did not differ between the LZ and DZ when the number of Tfr cells was normalized to the volume of each region (Fig. S1 G). In contrast, the vast majority of Tfr cells were found within 0–10 µm from the GC-mantle border (Fig. 1, E and F). It is possible that Tfr cells present in the GC modulate the engagement of Tfh-GC B cells in the LZ and the generation of autoreactive B cells in the DZ. However, their enrichment at the T-B and GC-mantle borders suggests an alternative model wherein Tfr cells regulate the antibody response from the outside in. For example, Tfr cells may prevent long-lived interactions between cognate T and B cells at the T-B border, a critical site for early Tfh differentiation (Qi et al., 2008; Kerfoot et al., 2011), or prevent activated Tfh cells from invading preexisting GC reactions (Shulman et al., 2013). Alternatively, Tfr cells may directly suppress B cells (Lim et al., 2005; Sage et al., 2016), preventing their differentiation into GC B cells, memory B cells, and/or long-lived plasma cells.

CXCR5, but not PD-1, expression levels correlate with localization of Tfr cells

Given the scarcity of Tfr cells in the GC, we sought to identify markers that could readily identify their location, analogous to the CXCR5^{Hi}PD-1^{Hi} phenotype described for GC Tfh cells (Crotty, 2011). Because CXCR5 enables T cell migration into the B cell follicle (Breitfeld et al., 2000), we first examined CXCR5 expression levels on Tfr cells in situ (Fig. 2, A–C). To enable multiplexing with CXCR5, and in later experiments CD69, Ki-67 was used to define the GC in place of BCL6. Tfr cells could be readily distinguished from Treg cells in the T cell zone by higher expression of CXCR5, but not the control marker CD20, on the population level and on the individual cell (Fig. 2, A–C). These data support the classification of CD3$^+$FOXP3$^+$CD25$^+$ T cells at the T-B border as Tfr cells and demonstrate the discriminating capacity of histo-cytometry. Based on their peripheral localization at the T-B border, we hypothesized that Tfr cells would express lower levels of CXCR5 than their nonregulatory counterparts. To address this question, we quantified the CXCR5 expression levels of Tfh (CD45RA$^-$CD3$^+$CD4$^+$CXCR5$^+$CD25$^-$FOXP3$^-$) and Tfr (CD45RA$^-$CD3$^+$CD4$^+$CXCR5$^+$CD25$^+$FOXP3$^+$) cells. Because PD-1 expression is used to define Tfh cells, we also separated the Tfr subsets into cells expressing PD-1 at three levels (negative [Neg], intermediate [Int], and high [Hi]) using flow cytometry (Fig. 2, D and E). Tfh cells expressed slightly higher levels of CXCR5 than their regulatory counterparts (Fig. 2 E). Furthermore, Tfr cells represented a small percentage (~4–22%) of total CXCR5$^+$ follicular T cells, Tfr and Tfh, regardless of PD-1 expression levels (Fig. S1 H).

We next assessed whether PD-1 expression levels correlated with the localization of these cells in situ. Using the mean fluorescence intensity (MFI) of PD-1, and the positional data gathered via histo-cytometry, we examined the spatial distribution of PD-1–expressing Tfh and Tfr cells (Fig. 2, F–H). The majority of Tfr cells were PD-1^{Neg} with only 1% of Tfr cells expressing high levels of PD-1 (Fig. 2 H). In contrast, ~34% of Tfh cells were PD-1^{Hi},

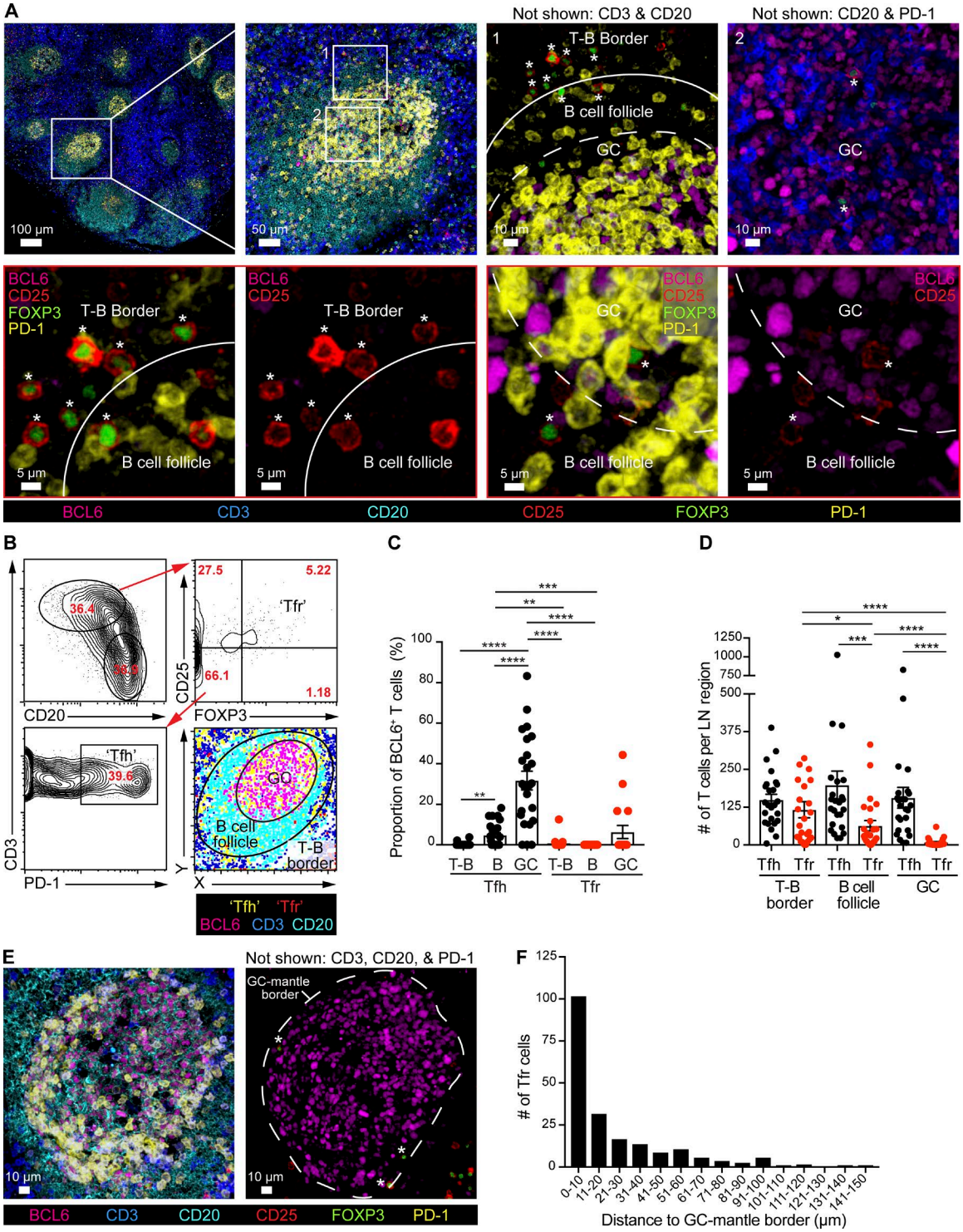

Figure 1. **Tfr cells are enriched at the T-B and GC-mantle borders of human mLNs.** Frozen sections were prepared from human mLNs and processed for confocal microscopy and histo-cytometry. **(A)** Images of LN sections depicting Tfh and Tfr (*) cells within CD20⁺ B cell follicles and BCL6⁺ GCs. **(B)** Histo-cytometry contour plots and gating strategy used to identify the distribution of Tfh and Tfr cells within the T-B border, B cell follicle, and GC. **(C)** Proportion of Tfh and Tfr cells that are BCL6⁺ as quantified by histo-cytometry (n = 24 follicles; four mLNs). **(D)** Number of Tfh and Tfr cells in distinct LN regions. Each symbol represents a LN region comparable to the images found in the second top panel in A, here and throughout. Data are pooled from 8–10 follicles per LN from three subjects (n = 26). **(E)** Confocal image of Tfr cells within a GC from a human mLN. **(F)** Distribution of Tfr cells within GCs. Data are pooled from five to nine GCs from four subjects, n = 27. Wilcoxon signed rank tests; mean ± SEM; *, P < 0.05; **, P < 0.01; ***, P < 0.001; ****, P < 0.0001.

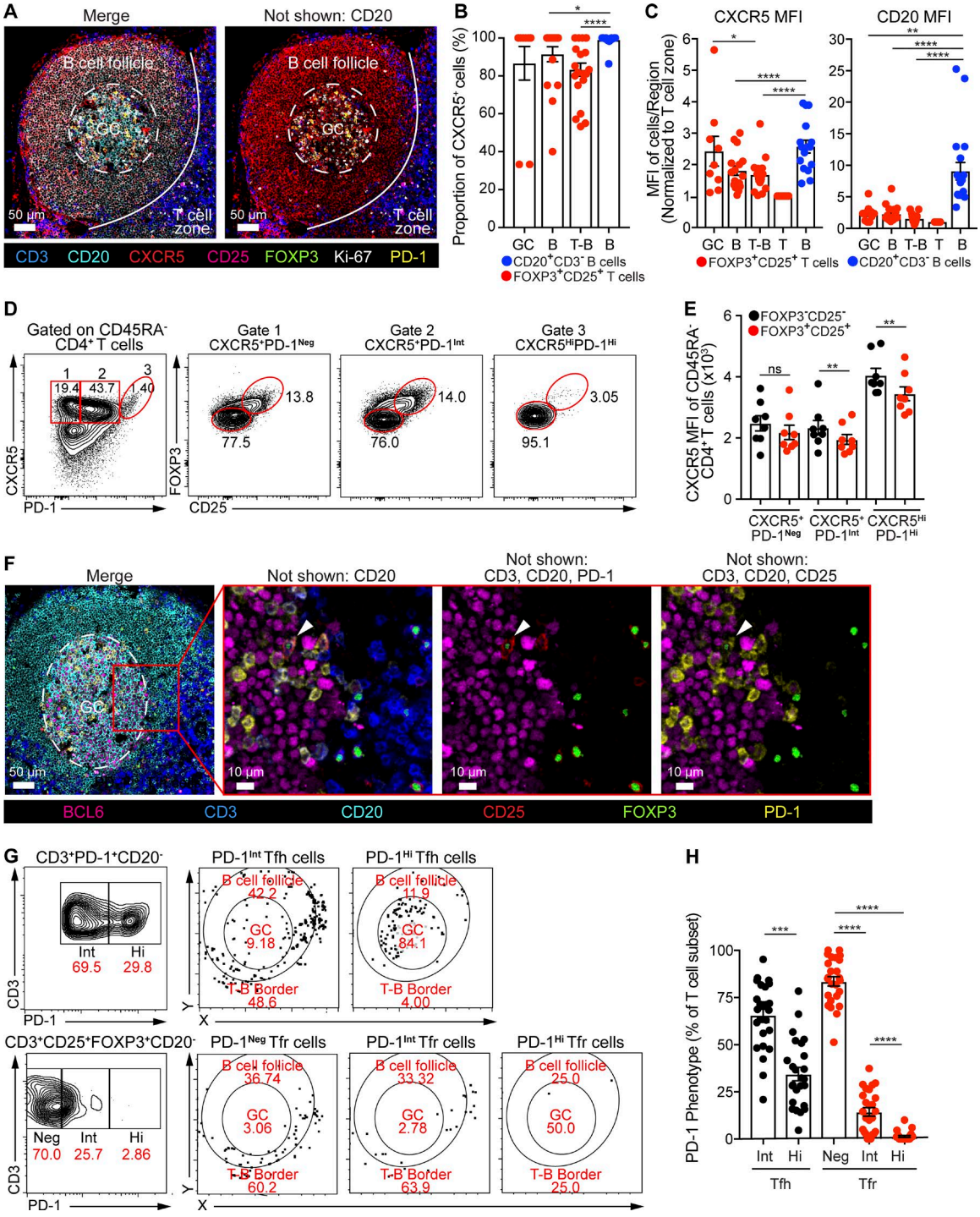

Figure 2. **CXCR5 expression levels correlate with localization of Tfr cells. (A)** Images depicting colocalization of CD20 and CXCR5. **(B)** Proportion of cells that are CXCR5$^+$ based on histo-cytometry gates drawn on CD3$^+$CD25$^+$FOXP3$^+$ cells in the T cell zone. **(C)** CXCR5 or CD20 MFIs for cell surfaces as quantified by histo-cytometry. CXCR5 and CD20 MFIs on cells from the GC, B cell follicle, "B," and T-B border (T-B) were normalized to MFIs from T cells present in the T cell zone (T) of the same image. **(B and C)** Each symbol represents data obtained from two to six images from four subjects (n = 24). **(D)** Flow cytometry gating strategy used to define populations in E. **(E)** CXCR5 MFI for FOXP3$^+$CD25$^+$ and FOXP3$^-$CD25$^-$ subsets gated in D, n = 8 subjects. **(F)** Images of rare PD-1$^+$ Tfr cell in the GC (arrowhead). **(G)** Histo-cytometry plots and gating strategy used to identify the phenotype and location of PD-1 expressing Tfh and Tfr cells. Each dot represents a cell surface. **(H)** Percentage of Tfh and Tfr subsets per image. Data are pooled from 8–10 follicles per LN from three subjects (n = 26). Wilcoxon signed rank tests; mean ± SEM; **, P < 0.01; ***, P < 0.001; ****, P < 0.0001.

and importantly, PD-1^{Hi} Tfh cells were significantly enriched in the GCs (Fig. 2 G and Fig. S1 I). Although the PD-1^{Hi} phenotype faithfully reported the location of GC Tfh cells, the relationship between PD-1 surface expression and Tfr cell location was less clear (Fig. 2 G and Fig. S1 I). We also evaluated surface expression of EBI2 (GPR183) on Tfr cells via flow cytometry. EBI2 is a

G-protein–coupled receptor that has been shown to direct T cells to the T-B border (Li et al., 2016). All FOXP3$^+$CD25$^+$ follicular T cell subsets expressed lower EBI2 levels than their nonregulatory counterparts with one exception: the CXCR5^{Hi}PD-1^{Hi} GC Tfh population (Fig. S1, J and K). Therefore, EBI2 is unlikely to account for retention of Tfr cells at the T-B border.

Tfr cells are transcriptionally more similar to Treg than Tfh cells

As PD-1 was heterogeneously expressed among human Tfr cells, we next evaluated whether PD-1 levels correlated with differences in the transcription of effector molecules. Because of the small number of PD-1^{Hi}CXCR5$^+$ follicular T cells present in mLNs, we isolated PD-1$^+$ Tfr and Tfh cells using a gate that encompassed both the PD-1^{Int} and PD-1^{Hi} populations, described as "PD-1$^+$ Tfr" or "Tfh" cells from this point on. Using surface CD25 and CD39 expression levels to define Treg cells (Mandapathil et al., 2009), T subsets were live sorted and gene expression was assessed using a Fluidigm Biomark panel of preselected genes involved in Tfh and Treg cell functions (Fig. 3 A and Fig. S2 A). A principal component analysis demonstrated that Tfr cells, regardless of PD-1 expression, had overlapping transcriptional profiles and more closely resembled Treg than Tfh cells (Fig. 3 B). Tfh cells had greater *BCL6* transcript (Fig. 3 C) and intracellular protein expression (Fig. 3, D and E) as compared with Tfr cells and Treg cells, whereas FOXP3 was abundantly expressed in all Treg cells (Fig. 3, C–E). We also examined differences in the expression of ICOS and CTLA-4, an important negative regulator constitutively expressed on Treg cells (Hori et al., 2003), and found that PD-1$^+$ Tfr cells had higher levels of ICOS and CTLA-4 protein than PD-1^{Neg} Tfr cells (Fig. 3 E). Several other transcription factors and effector molecules important for Tfh and/or Treg cell differentiation and function were examined using RT-PCR (*MAF*, *IL-10*, *IL-21*, *IRF4*, *TIGIT*, *GARP*; Tran et al., 2009; Cretney et al., 2011; Kroenke et al., 2012; Locci et al., 2013; Joller et al., 2014; Wu et al., 2016; Fig. S2, B–G). Of note, *GARP*—a molecule shown to control surface expression of latent TGF-β on activated human Treg cells (Tran et al., 2009)—was increased on both subsets of Tfrs as compared with the Tfh and Treg cell populations (Fig. S2 G).

Functional characteristics and suppressive capacity of Tfr cells

To relate these transcriptional data demonstrating that PD-1$^+$ and PD-1^{Neg} Tfr cells more closely resembled Treg than Tfh cells, we next assessed the capacity of Tfr cells to express IL-10, IL-21, or CD40L as well as their ability to suppress Tfh-mediated B cell antibody production in vitro, the gold standard in the field. LN cells were incubated with PMA/ionomycin in the presence of monensin for 4.5 h, and intracellular IL-10 and IL-21 levels were quantified by flow cytometry (Fig. 4, A–C). Consistent with our RT-PCR analyses, we observed a higher percentage of IL-10–producing cells in the PD-1$^+$ Tfr cell population as compared with the other T cell subsets (Fig. 4 B). IL-21, the prototypical Tfh cytokine (Crotty, 2011), was primarily produced by Tfh cells (Fig. 4 C). Recently, Tfr cell–derived IL-10 has been shown to support B cell differentiation in a mouse model of acute viral infection (Laidlaw et al., 2017). Given the scarcity of Tfr cells present in the GCs of human mLNs, it is unlikely that this population exerts a dominant effect over the more plentiful population of IL-10–producing Tfh cells found there. Nonetheless, it is possible that Tfr and Treg cell–derived IL-10 modulates humoral immunity by fine-tuning the B cell response elsewhere. In addition to cytokines, CD40-CD40L signaling is critical for B cell activation, proliferation, and differentiation (Crotty, 2011). After stimulation with PMA/ionomycin, 60% of Tfh cells expressed CD40L protein as compared with ∼12–20% of the regulatory subsets (Fig. 4, D and E).

To evaluate Tfr-mediated suppression of antibody production, purified Tfh and PD-1$^+$ Tfr cells were incubated with allogeneic naive B cells for 7 d in the presence of staphylococcal enterotoxin B (SEB) in a 3:1:1 ratio (Tfh/PD-1$^+$ Tfr/B cells). SEB-stimulated B cells produced significant amounts of IgG, and 10-fold less IgA, when incubated with Tfh cells at a 3:1 ratio; however, IgG and IgA levels decreased by more than 95% and 70%, respectively, when PD-1$^+$ Tfr cells were added to the cultures (Fig. 4, F and G). Using a T cell–free culture system, Lim et al. (2005) demonstrated that human Treg cells could directly suppress B cells. We used a similar strategy and found that PD-1$^+$ Tfr cells reduced IgG secretion by more than 40% when incubated with B cells cultured in the presence of anti-IgM/IgG, rCD40L, and cytokines (IL-4/IL-21; Fig. 4 H).

After studies showing that mouse PD-1–deficient Tfr cells were more suppressive than wild-type Tfr cells (Sage et al., 2013), we directly compared the per cell potency of Treg, PD-1^{Neg} Tfr, and PD-1$^+$ Tfr cells at 3:1 and 9:1 ratios (Tfh/regulatory subset; Fig. 4 I). All regulatory subsets significantly inhibited Tfh-induced IgG production by B cells at 3:1 and 9:1 ratios (statistics not shown). However, the efficiency of this suppression was largely dependent on the number of regulatory cells, relative to Tfh cells, present in the cultures (Fig. 4 I). Together, these results demonstrate that suppression of antibody production is not restricted to Tfr cells in vitro, but instead requires a sufficient number of regulatory cells for an inhibitory effect, an observation with direct bearing on our interpretation of the Tfr cell localization data obtained using histo-cytometry.

CD69$^+$ Tfr cells express suppression-associated molecules and associate with CD69$^+$ T cells at the T-B border

Although our in vitro assays demonstrate the functional potential of Tfr cells, there is no evidence that such assays reflect Tfr-mediated suppression in vivo. Moreover, many of the mechanisms proposed for Tfr-mediated suppression—down-regulation of costimulatory molecules by Tfr-expressed CTLA-4, cytolysis of Tfh or GC B cells, or mechanical disruption of Tfh-B conjugates—depend on direct cell contacts in the LN microenvironment (Sage et al., 2014; Wing et al., 2014; Sage and Sharpe, 2015). To determine where Tfr cells are mediating their suppression, we examined the distribution and nearest neighbors of Tfr cells expressing CD69, a marker associated with tissue residency that is up-regulated in response to activation (Ziegler et al., 1994; Masopust and Schenkel, 2013; Bremser et al., 2015; Ashouri and Weiss, 2017; Fig. 5 A). In mice, CD69-expressing Treg cells correspond to a highly suppressive subset of Treg cells with elevated expression of TGF-β and activation-associated markers such as CTLA-4, ICOS, and pSTAT5 (Cortés et al., 2014). Accordingly, a significant proportion of CD69$^+$ Treg cells in the LNs expressed

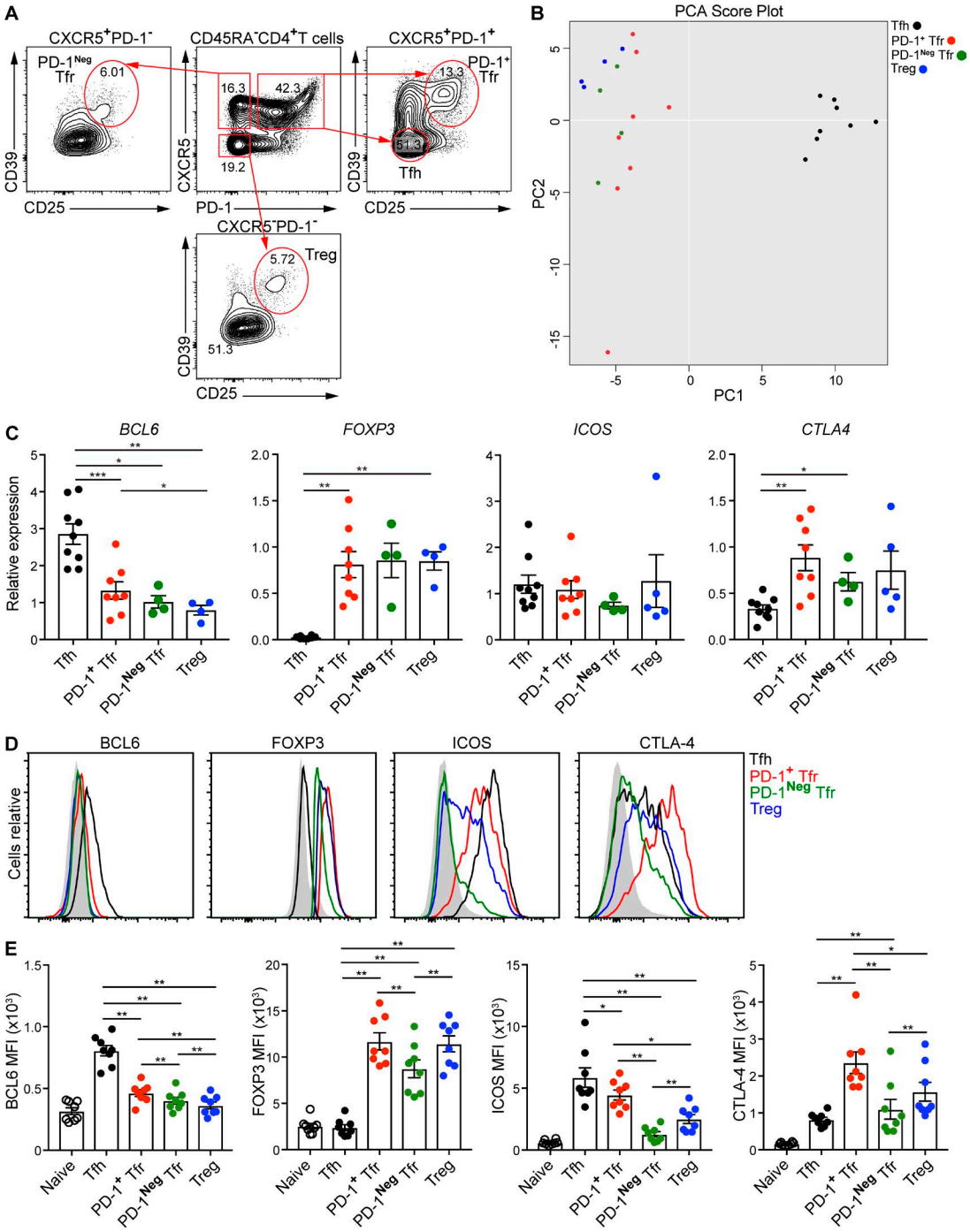

Figure 3. **Characterization of Tfh, Tfr, and Treg cell populations. (A)** Sorting strategy used for the transcriptome analysis of Tfh, Tfr, and Treg cell subsets. **(B)** Principal component analysis showing the distribution of Tfh, PD-1⁺ Tfr, PD-1^{Neg} Tfr, and Treg cells for the first two principal components. PC1 accounts for just over 50% of the variance whereas PC2 accounts for 20%. **(C)** Relative mRNA expression of *BCL6, FOXP3, ICOS,* and *CTLA4* determined by RT-PCR for the sorted populations in A. Data are from nine subjects, but cells were not sufficient for analysis in all subsets for every subject. **(D)** Histograms showing the MFI for BCL6, FOXP3, ICOS, and CTLA-4; naive CXCR5⁻CD45RA⁺CD4⁺ T cells (gray histograms). **(E)** MFI for BCL6, FOXP3, ICOS, and CTLA-4 obtained by flow cytometry (n = 8 subjects). Naive CXCR5⁻CD45RA⁺CD4⁺ T cells were included as a baseline but were not included in the statistical analyses. Paired t tests; mean ± SEM; *, P < 0.05; **, P < 0.01; ***, P < 0.001.

elevated levels of surface CD38, CTLA-4, and GARP at steady-state (Fig. S3). The CD69⁺ status of Tfrs was relatively consistent across all LN regions with ∼59, 56, and 46% of Tfrs expressing CD69 in the T-B border, B cell follicle, and GC, respectively (Fig. 5 B). CD69⁺ Tfrs were significantly associated with CD69⁺ T cells at the T-B border, whereas CD69⁻ Tfr cells were more frequently found in close contact with CD3⁺CD69⁻ T cells and CD20⁺ B cells (Fig. 5 C). These observations are in agreement with previous studies demonstrating that Treg cells do not prevent T cell activation but instead limit effector function after stimulatory

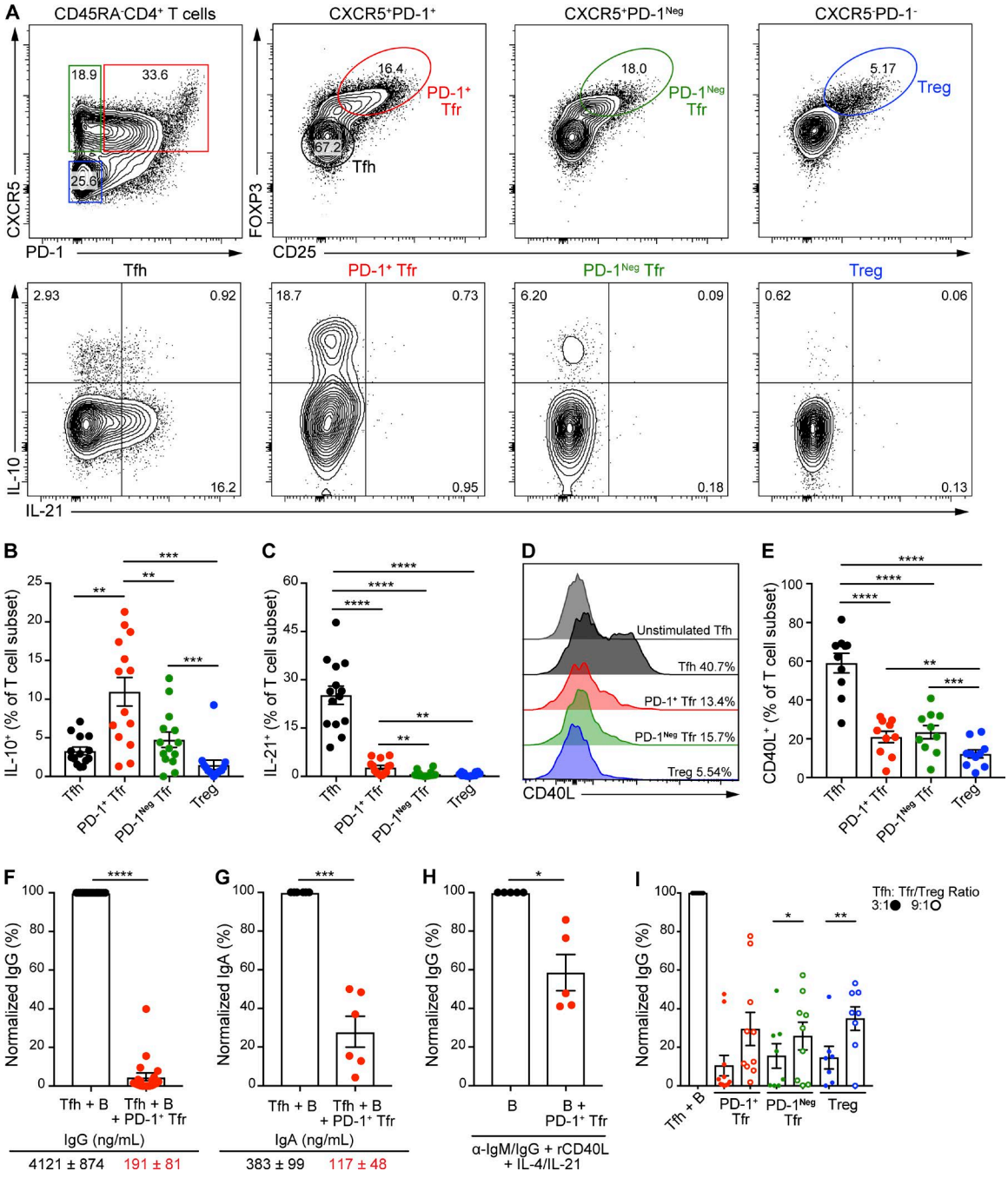

Figure 4. **PD-1⁺ and PD-1^{Neg} Tfr cells suppress antibody responses in vitro. (A)** Flow cytometry plots showing the percentage of cells producing IL-10 or IL-21 within the indicated populations. All cells were first gated on live CD4⁺CD45RA⁻ T cells (not depicted), then CXCR5 and PD-1, and followed by FOXP3 and CD25. LMNCs were activated with PMA/ionomycin. Unstimulated controls were used to draw cytokine gates. Percentage of IL-10 (B) or IL-21 (C) producing cells within T cell subsets as determined by flow cytometry and gated in A. Data are pooled from three similar experiments, *n* = 14 subjects. **(D)** CD40L flow cytometry histograms. **(E)** Percentage of T cells that are CD40L⁺ based on gates drawn on unstimulated controls. Data are pooled from two similar experiments, *n* = 10 subjects. Analysis of IgG (F) or IgA (G) secretion by ELISA after stimulation with SEB in coculture with a 3:1 ratio of Tfh cells and B cells or 3:1:1 ratio of sorted Tfh cells, PD-1⁺ Tfr cells, and B cells for 7 d; *n* = 19 subjects (F) or *n* = 6 subjects (G). **(H)** IgG secretion from Tfh cell–free coculture experiments using mitogen-activated B cells with or without PD-1⁺ Tfr cells at a 1:1 ratio; *n* = 5. **(I)** IgG secretion using sorted Tfh, PD-1⁺ Tfr cells, PD-1^{Neg} Tfr cells, or Treg cells at indicated ratios for 7 d *n* = 6–10 subjects. Not depicted: Differences between the "Tfh + B" and all other groups were highly significant. For F–I, antibody concentrations are expressed as a percentage of the corresponding "Tfh + B" group titers. Paired *t* tests; mean ± SEM; *, P < 0.05; **, P < 0.01; ***, P < 0.001; ****, P < 0.0001.

TCR signaling (Mempel et al., 2006; Liu et al., 2015). Furthermore, Sage et al. demonstrated that mouse Tfr cells allowed initial activation of B cells, marked by up-regulation of CD69, but suppressed downstream effector responses in both B cells and Tfh cells (Sage et al., 2016). Of note, Tfr-mediated suppression resulted in sustained inhibition and epigenetic changes in B cells, supporting our interpretation that Tfr cells do not need to physically reside in the GC to modulate antibody production.

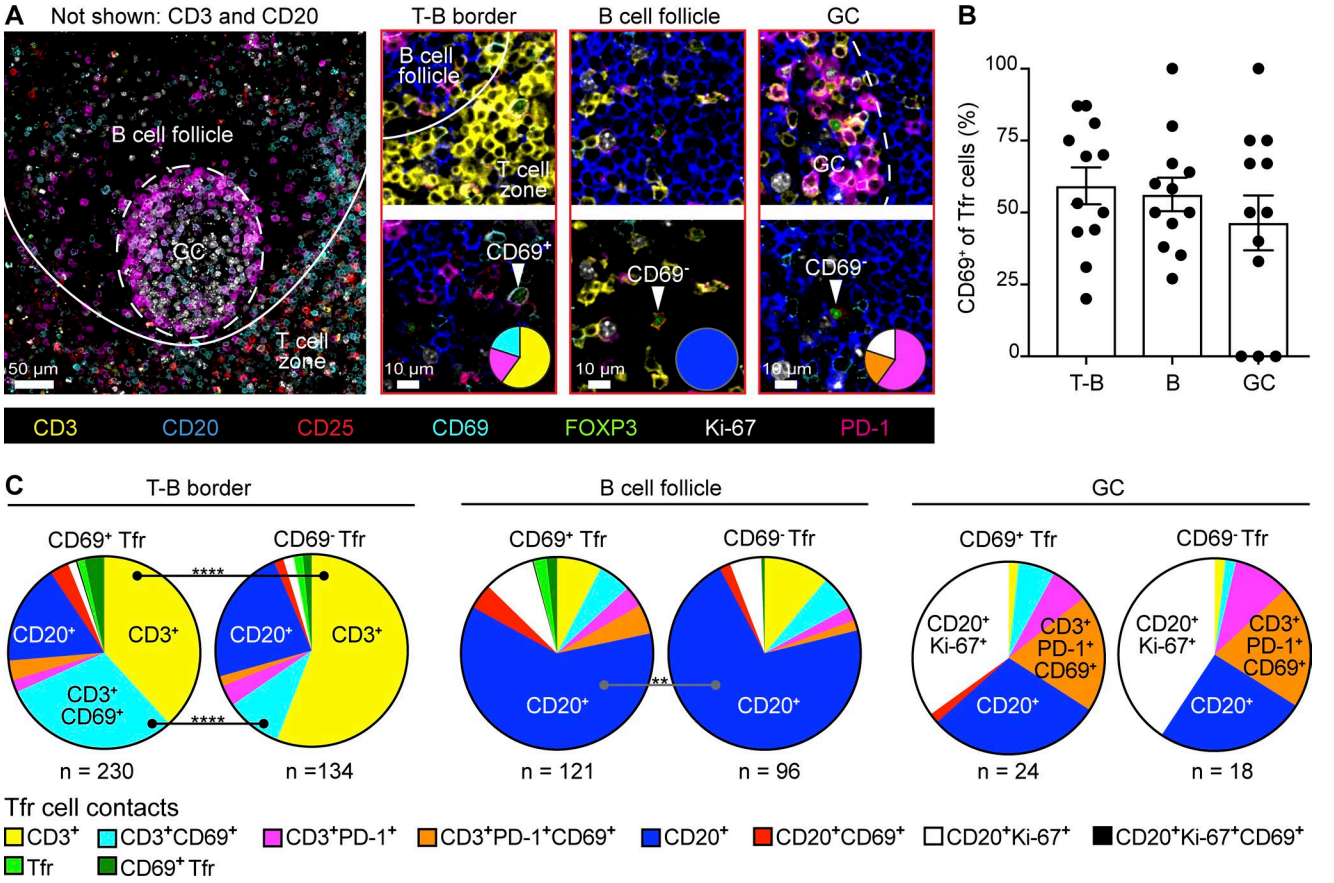

Figure 5. **Location and phenotype of Tfr cell contacts in situ. (A)** Images of mLN sections depicting the phenotype and close cellular contacts of Tfr cells (arrowheads) at the T-B border, B cell follicle, or GC. Pie graphs denote the phenotype of the cells in direct contact with Tfr cells. Color legend is the same as in C. **(B)** Percentage of $CD69^+$ Tfrs of total Tfr cells per LN region. Data are pooled from three to five follicles per LN from three subjects; $n = 12$; mean ± SEM. **(C)** Phenotype of cells in direct contact with $CD69^+$ or $CD69^-$ Tfr cells at the T-B border, B cell follicle, or GC. Data are plotted as mean percentages of cell contacts. Number of Tfr cells examined per phenotype and LN region is denoted underneath each pie chart. Paired *t* tests; **, $P < 0.01$; ****, $P < 0.0001$.

In summary, our data provide a detailed description of the spatial distribution, functional characteristics, and suppressive capacity of Tfr cells in human LNs. In addition to identifying a population of $PD\text{-}1^{Neg}$ Tfr cells, our imaging and flow cytometry studies demonstrate that Tfh cells far outnumber Tfr cells, especially in the GCs. The enrichment of $CD69^+$ Tfr cells at the T-B border and the ability of these cells to express GARP, a protein critical for the surface expression of latent TGF-β in activated human Treg cells (Tran et al., 2009), suggest that Tfr cells may modulate the antibody response in a TGF-β–dependent manner at this anatomical site. It is noteworthy that TGF-β signaling in T cells has been shown to prevent Tfh accumulation in the follicles and autoantibody production in mouse studies (McCarron and Marie, 2014). We speculate that CD69 expression, along with CXCR5, enables activated Tfr cells to be maintained at the T-B and GC-mantle borders, where they act as immunosuppressive gatekeepers to restrict differentiation, entry, and function of Tfh and B cells in reactive LNs. Our findings challenge the widely held paradigm that Tfr cells function within the GC and instead suggest a model where Tfr cells regulate the humoral immune response from the "outside in." Because of their discrete localization at the T-B border, we propose the nomenclature Tfr-T/B to distinguish these cells from intrafollicular Tfr cells while acknowledging that live imaging studies are required to assess the in vivo behavior of Tfr-T/B cells.

Materials and methods

LNs and cells

mLNs were obtained as discarded tissue in nonmalignancy surgeries from the Cleveland Clinic and University Hospitals of Cleveland. The LNs were crushed and filtered using 75-µm cell strainers. LNs were obtained and processed on the same day and cryopreserved in liquid nitrogen. The project was reviewed and approved by the University Hospitals Cleveland Medical Center and Cleveland Clinic Institutional Review Boards. Blood was obtained to make peripheral blood mononuclear cells and subsequently B cells from healthy subjects (University Hospitals Cleveland Medical Center Institutional Review Board No. 07-07-22). All samples were obtained after informed consent except the deidentified, discarded tissue samples that were deemed exempt human research by the Institutional Review Board. Confocal microscopy and histo-cytometry data were calculated from seven mLNs from five different subjects. Flow cytometry, RT-PCR, and cell suppression assay data were obtained from mLNs from 50 subjects. In total, mLNs from 55 different subjects were examined.

Immunohistochemistry and confocal microscopy

mLNs were harvested and fixed with CytoFix/CytoPerm (BD Biosciences) diluted in PBS (1:4) for 5 d. After fixation, tissues were washed for 2 d in PBS and incubated in 30% sucrose for 5 d before embedding in OCT compound (Tissue-Tek). 30-µm sections were cut on a CM3050S cryostat (Leica) and adhered to Super Frost Plus Gold slides (Electron Microscopy Services). Frozen sections were permeabilized and blocked for 1–2 h in PBS containing 0.3% Triton X-100 (Sigma-Aldrich), 1% bovine serum albumin, and 1% human Fc block. Sections were stained with directly conjugated antibodies for 12 h at 4°C in a humidity chamber in the dark. The following antibodies were used for confocal imaging of human mLNs: anti-BCL6 (K112-91; BD Biosciences), anti-CD3 (UCHT1; BioLegend), anti-CD4 (polyclonal goat; R&D), anti-CD20 (L26; eBioscience), anti-CD25 (CD25-4E3; eBioscience), anti-CD35 (E11; BioLegend), anti-CXCR5 (RF8B2; BD Biosciences), anti-CD69 (FN50; BioLegend), anti-FOXP3 (236A/E7; eBioscience), anti–Ki-67 (B56; BD Biosciences), and anti–PD-1 (EH12.2H7; BioLegend). Cell nuclei were visualized with JOJO-1 (Thermo Fisher Scientific). Stained slides were mounted with Fluoromount G (eBioscience) and sealed with a glass coverslip. Representative sections from different mLNs were acquired using a SP8 confocal microscope (Leica) equipped with a 40× objective (NA 1.3), two HyD and three photomultiplier tube detectors, and six lasers (UV, Argon, DPSS 561, OHeNe, HeNe, and 690 Diode) capable of nine excitation wavelengths (405, 458, 476, 488, 514, 561, 594, 633, and 690 nm). All images were captured at an 8-bit depth, with a line average of 3, and 1,024 × 1,024 format with the following pixel dimensions: x (0.284–0.378 µm), y (0.284–0.378 µm), and z (1–1.25 µm).

Histo-cytometry

For histo-cytometric analysis of Tfh and Tfr cells, a seven- to eight-color panel was developed consisting of the following fluorophores: BV421, BV510, AF488, JOJO-1, PE, AF594, AF647, and AF700. Fluorophore emission was collected on separate detectors with sequential laser excitation of compatible fluorophores (three to four per sequential) used to minimize spectral spillover. The Channel Dye Separation module within the LASX 1.6 software (Leica) was then used to correct for any residual spillover. Threshold identification, voxel gating, surface creation, and masking were performed as previously described (Gerner et al., 2012, 2015; Liu et al., 2015; Radtke et al., 2015). For publication quality images, Gaussian filters, brightness/contrast adjustments, and channel masks were applied uniformly to all images. Images are presented as maximum intensity projections of tiled z-stacks. Histo-cytometric quantification of cell surfaces was based on images with unadjusted gamma values. Cells were segmented on JOJO-1$^+$ nuclei and used to create surfaces. Channel statistics for all surfaces were exported into Excel (Microsoft) and converted to a csv file for direct visualization in FlowJo v10.1r5 (Treestar). Mean voxel intensities for all channels were plotted and used for gating distinct lymphocyte populations. The T-B border was defined as the region extending 50 µm around the B cell follicle. B cell follicle and GC gates were defined using positional data on the CD20$^+$ and BCL6$^+$/Ki-67$^+$ surfaces, respectively. To calculate the density of Tfr cells per GC region, the surface function in Imaris was used to create volumetric surfaces. The number of Tfr cells was then divided by the volumes obtained from these regions. The measurement tool in Imaris was used to calculate the distance from the Tfr centroid to the GC-mantle border. CXCR5 levels were normalized to CXCR5 expression on T cells in the T cell area to control for variations in laser intensities resulting from image acquisitions on separate days. Tfr-cell contacts were defined as cells in direct contact with Tfr cells based on voxel overlap of membrane stains. Cell phenotypes were defined using fluorescence intensities above background for the CD3, CD20, CD25, CD69, FOXP3, Ki-67, and PD-1 channels. If a particular Tfr cell was found to be in contact with two CD3$^+$ cells, one CD3$^+$PD-1$^+$ cell, and three CD20$^+$ cells, then its cell contacts would be 33.3% CD3$^+$, 16.7% CD3$^+$PD-1$^+$, and 50% CD20$^+$. These percentages were averaged across Tfr cells per respective region and used to compute the pie charts in Fig. 5. Ki67$^+$CD3$^+$ or CD25$^+$CD3$^+$ cells were placed into the CD3$^+$ bin, whereas CD69$^+$Ki-67$^+$CD3$^+$ or CD69$^+$CD25$^+$CD3$^+$ cells were placed into the CD3$^+$CD69$^+$ bin. All of these subsets were present at low frequencies. Ki-67$^+$ Tfr cells represented only 4% of the total Tfrs examined (25/621) with 92% of these observed from one subject.

Flow cytometry

mLNs were thawed and stained for surface and intracellular markers. The following antibodies and dyes were used: Aqua LIVE/DEAD (Invitrogen); anti-CD27 AF700 (O323; BioLegend) or BV711 (M-T271; BD Biosciences); anti–PD-1 BV421 (EH12.2H7; BioLegend), anti–CD4 APC/Cy7 (RPA-T4; BioLegend), or BV650 (SK3; BD Biosciences); anti-CXCR5 PE/Dazzle (J252D4; BioLegend); anti-CD39 FITC (A1; BioLegend); anti-CD45RA BV650 or FITC (HI100; BD Biosciences); anti-CD25 PE/Cy7 or BV605 (BC96; BioLegend); anti-CD3 BUV395 (UCHT1; BD Biosciences); anti-ICOS BV711 (DX29; BD Biosciences); anti–CTLA-4 PE/Cy5 (BNI3; BD Biosciences); anti-CD69 APC/Fire 750 (FN50; BioLegend); anti-GARP PE/Cy7 (7B11; BioLegend); anti-CD38 AF700 (HIT2; eBioscience); anti-FOXP3 PE (259D/C7; BD Biosciences) or APC (PCH101; eBioscience); anti-BCL6 AF647 (K112-91; BD Biosciences); anti–IL-10 PE-Dazzle (JES3-9D7; BioLegend); anti–IL-21 AF647 (3A3-N2.1; BD Biosciences); and anti-CD40L BV421 (21–34; BioLegend). For phenotypic characterization experiments, permeabilization was performed using the FOXP3 Fixation/Permeabilization Concentrate and Diluent kit (eBioscience), and intracellular stainings were done. For IL-10 and IL-21 staining, LN cell suspensions were stimulated for 4.5 h in the presence of PMA/ionomycin (50 ng/ml and 1 µg/ml, respectively) or left unstimulated as a control in RPMI 1640 medium supplemented with 10% FCS. Monensin (BD Biosciences) was added at the beginning of stimulation. Cells were fixed for 60 s with 1% paraformaldehyde before permeabilization with the FOXP3 Fixation/Permeabilization Concentrate and Diluent kit, followed by intracellular staining for 1 h. Cells were resuspended in 1% paraformaldehyde until acquisition on a Fortessa or Symphony A5 cytometer (BD Biosciences) and analyzed using FlowJo.

For Fig. 2 (D and E), Fig. S1 (H, J, and K), and Fig. S3, live CD45RA$^-$ cells were defined as follows: PD-1^{Int} Tfh (CXCR5$^+$PD-1^{Int}CD25$^-$FOXP3$^-$), PD-1^{Hi} Tfh (CXCR5$^+$PD-1^{Hi}CD25$^-$FOXP3$^-$), PD-1^{Neg} Tfr (CXCR5$^+$PD-1$^-$CD25$^+$FOXP3$^+$), PD-1^{Int} Tfr

($CXCR5^+PD\text{-}1^{Int}CD25^+FOXP3^+$), PD-$1^{Hi}$ Tfr ($CXCR5^+PD\text{-}1^{Hi}CD25^+FOXP3^+$), Treg ($CXCR5^-PD\text{-}1^-CD25^+FOXP3^+$), and naive T cells ($CD45RA^+CXCR5^-CD25^-FOXP3^-$). In Fig. 3 (D and E) and Fig. 4 (A–E), T cell subsets were defined as above except for Tfh ($CXCR5^+PD\text{-}1^{Int/Hi}CD25^-FOXP3^-$) and PD-$1^+$ Tfr cells ($CXCR5^+PD\text{-}1^{Int/Hi}CD25^+FOXP3^+$). For Fig. 3 (A–C), Fig. 4 (F–I), and Fig. S2, $CD45RA^-$ cells were live-sorted based on the following marker expression: PD-1^+ Tfr ($CXCR5^+PD\text{-}1^{Int/Hi}CD25^+CD39^+$), PD-$1^{Neg}$ Tfr ($CXCR5^+PD\text{-}1^{Neg}CD25^+CD39^+$), Tfh ($CXCR5^+PD\text{-}1^{Int/Hi}CD25^-CD39^-$), and Treg cell ($CXCR5^-PD\text{-}1^-CD25^+CD39^+$). The majority (>86%) of $CD25^+CD39^+$ T cells isolated using this gating strategy were $FOXP3^+$.

Real-time quantitative RT-PCR

RNA was first isolated from sorted cell populations using the RNeasy Micro Plus kit (Qiagen). Then, each sample was reverse-transcribed using Reverse Transcription Mastermix (Fluidigm). cDNA was amplified with 15 cycles of specific target preamplification using the Fluidigm Pre-Amp Master Mix and the full complement of primers. Preamplified samples were subjected to an exonuclease reaction, using Exonuclease I and Exonuclease I Reaction Buffer (New England Biolabs). Samples were then diluted 1:5 with TE buffer (Thermo Fisher Scientific). An aliquot of each of the diluted, preamplified samples was then mixed with SsoFast EvaGreen Supermix with Low Rox (Bio-Rad) and DNA Binding Dye Sample Loading Reagent (Fluidigm). Assays were prepared using 100-µM primers combined with 2× Assay Loading Reagent (Fluidigm) and DNA suspension buffer (TEKnova), for a final primer concentration of 5 µM. Samples and assays were plated into a primed Biomark 96.96 quantitative PCR DynamicArray microfluidic chip, and quantitative PCR was run on the Biomark HD system.

B cell coculture assays

Sorted $CD4^+$ T cell subsets were plated with purified allogeneic naive B cells (Naive B cell Isolation kit; STEMCELL Technologies) in a 3:1 ratio and cocultured for 7 d in the presence or absence of SEB (0.1 µg/ml; Toxin Technology Inc.). The B cells were from a single stock of purified naive B cells to allow for a consistent readout of Tfh and Tfr activity on antibody production. Because allogeneic B cells were used, the mitogen SEB was used to induce a signal substantially above the allogeneic reaction alone. The coculture system with just the allogeneic stimulus alone (no SEB) results in <5% IgG levels. A low dose of SEB was selected because our preliminary experiments demonstrated that this concentration induced a subplateau amount of antibody production, thus allowing for a greater window of Tfr-mediated effects on the Tfh and B cell response. Different ratios of Tfh/Tfr cells (3:1 and 9:1) were used, but B/Tfh cell ratios were kept constant. For quantification of antibody production in vitro, total IgG was quantified in culture supernatants with a total anti-IgG capture antibody (1010-01; Southern Biotech) and alkaline phosphatase–conjugated anti–total IgG detection antibody (1030-04; Southern Biotech). In control experiments, appreciable IgG levels were not detected in coculture experiments without Tfh cells. In addition, the following conditions generated IgG titers below the level of detection: PD-1^+ Tfr + SEB-stimulated B cells, nonfollicular $CXCR5^-CD45RA^-CD4^+$ T cells + SEB-stimulated B cells, nonfollicular $CXCR5^-CD45RA^+CD4^+$ T cells + SEB-stimulated B cells, Tfh + B cells (no SEB), and SEB-stimulated B cells alone ($n > 3$ subjects).

For T cell–free B cell stimulation, purified allogeneic naive B cells were cultured with anti-IgM/IgG (1 µg/ml; Jackson Immunoresearch), recombinant CD40L (5 µg/ml; BioLegend), 20 ng/ml IL-4 (Peprotech), and 40 ng/ml IL-21 (Peprotech) for 7 d. Sorted regulatory cell subsets were incubated at a 1:1 ratio with activated allogeneic naive B cells for 7 d in the presence of SEB (0.5 µg/ml). Total IgG was quantified in culture supernatants with AffiniPure F(ab′)2 Fragment goat anti–human IgG + IgM (H+L; Jackson ImmunoResearch) and biotin–conjugated anti–total IgG detection antibody (Jackson ImmunoResearch). To avoid potential "masking" artifacts resulting from stimulation and detection with an anti-IgG antibody, normalized and not absolute IgG titers were reported (Fig. 4 H). IgA was quantified using IgA human ELISA kits (Thermo Fisher Scientific).

Statistical analysis

Statistical analysis was performed using Prism 7 (GraphPad). Differences between two groups were compared using paired *t* tests or Wilcoxon matched-pairs signed rank tests for nonnormal distributions (ns; *, $P < 0.05$; **, $P < 0.01$; ***, $P < 0.001$; and ****, $P < 0.0001$). All figures show the mean ± SEM unless otherwise noted. For quantification of the imaging data, each symbol represents a LN region comprised of a GC, B cell follicle, T-B border, and 50 µm region including the T cell zone. Differences between groups were not significant unless stated otherwise.

Online supplemental information

Fig. S1 provides data on the proportion of $CD3^+CD25^+FOXP3^+$ cells that are $CD4^+$, $BCL6^+$, and $CD25^+$, the distribution of Tfr cells in the LZ and DZ of the GC, the frequency and location of PD-1–expressing Tfh and Tfr cells, and the expression of EBI2 among Tfh and Tfr cells. Fig. S2 shows a heat map and RT-PCR data comparing the gene expression profiles of Treg, Tfh, and Tfr cells. Fig. S3 includes data on the surface expression of CD38, CTLA-4, and GARP among various $CD4^+$ T cell populations.

Acknowledgments

We would like to thank Dr. Luis Franco for his assistance with statistical analysis.

This research was supported by the National Institutes of Health (AI108972, AI036219, UL1TR000439, AI114852), Veterans Affairs, University Hospitals and Cleveland Clinic Tissue Procurement and the Intramural Research Program, and the National Institute of Allergy and Infectious Diseases, National Institutes of Health (to A.J. Radtke and R.N. Germain).

The authors declare no competing financial interests.

Author contributions: A.J. Radtke, I. Sayin, and D.H. Canaday designed the experiments, analyzed the results, and wrote the manuscript. L.A. Vella, R.S. Herati, and W. Jin performed and analyzed experiments. R.N. Germain, M. Buggert, M.R. Betts, and E.J. Wherry helped analyze data and write the manuscript.

Submitted: 25 October 2017
Revised: 2 March 2018
Accepted: 1 May 2018

References

Ashouri, J.F., and A. Weiss. 2017. Endogenous Nur77 is a specific indicator of antigen receptor signaling in human T and B cells. *J. Immunol.* 198:657–668. https://doi.org/10.4049/jimmunol.1601301

Breitfeld, D., L. Ohl, E. Kremmer, J. Ellwart, F. Sallusto, M. Lipp, and R. Förster. 2000. Follicular B helper T cells express CXC chemokine receptor 5, localize to B cell follicles, and support immunoglobulin production. *J. Exp. Med.* 192:1545–1552. https://doi.org/10.1084/jem.192.11.1545

Bremser, A., M. Brack, and A. Izcue. 2015. Higher sensitivity of Foxp3+ Treg compared to Foxp3- conventional T cells to TCR-independent signals for CD69 induction. *PLoS One.* 10:e0137393. https://doi.org/10.1371/journal.pone.0137393

Chowdhury, A., P.M. Del Rio Estrada, G.K. Tharp, R.P. Trible, R.R. Amara, A. Chahroudi, G. Reyes-Teran, S.E. Bosinger, and G. Silvestri. 2015. Decreased T follicular regulatory cell/T follicular helper cell (TFH) in Simian Immunodeficiency Virus-infected Rhesus macaques may contribute to accumulation of TFH in chronic infection. *J. Immunol.* 195:3237–3247. https://doi.org/10.4049/jimmunol.1402701

Chung, Y., S. Tanaka, F. Chu, R.I. Nurieva, G.J. Martinez, S. Rawal, Y.H. Wang, H. Lim, J.M. Reynolds, X.H. Zhou, et al. 2011. Follicular regulatory T cells expressing Foxp3 and Bcl-6 suppress germinal center reactions. *Nat. Med.* 17:983–988. https://doi.org/10.1038/nm.2426

Cortés, J.R., R. Sánchez-Díaz, E.R. Bovolenta, O. Barreiro, S. Lasarte, A. Matesanz-Marín, M.L. Toribio, F. Sánchez-Madrid, and P. Martín. 2014. Maintenance of immune tolerance by Foxp3+ regulatory T cells requires CD69 expression. *J. Autoimmun.* 55:51–62. https://doi.org/10.1016/j.jaut.2014.05.007

Cretney, E., A. Xin, W. Shi, M. Minnich, F. Masson, M. Miasari, G.T. Belz, G.K. Smyth, M. Busslinger, S.L. Nutt, and A. Kallies. 2011. The transcription factors Blimp-1 and IRF4 jointly control the differentiation and function of effector regulatory T cells. *Nat. Immunol.* 12:304–311. https://doi.org/10.1038/ni.2006

Crotty, S. 2011. Follicular helper CD4 T cells (TFH). *Annu. Rev. Immunol.* 29:621–663. https://doi.org/10.1146/annurev-immunol-031210-101400

Crotty, S. 2014. T follicular helper cell differentiation, function, and roles in disease. *Immunity.* 41:529–542. https://doi.org/10.1016/j.immuni.2014.10.004

Gerner, M.Y., W. Kastenmuller, I. Ifrim, J. Kabat, and R.N. Germain. 2012. Histo-cytometry: a method for highly multiplex quantitative tissue imaging analysis applied to dendritic cell subset microanatomy in lymph nodes. *Immunity.* 37:364–376. https://doi.org/10.1016/j.immuni.2012.07.011

Gerner, M.Y., P. Torabi-Parizi, and R.N. Germain. 2015. Strategically localized dendritic cells promote rapid T cell responses to lymph-borne particulate antigens. *Immunity.* 42:172–185. https://doi.org/10.1016/j.immuni.2014.12.024

Hori, S., T. Nomura, and S. Sakaguchi. 2003. Control of regulatory T cell development by the transcription factor Foxp3. *Science.* 299:1057–1061. https://doi.org/10.1126/science.1079490

Joller, N., E. Lozano, P.R. Burkett, B. Patel, S. Xiao, C. Zhu, J. Xia, T.G. Tan, E. Sefik, V. Yajnik, et al. 2014. Treg cells expressing the coinhibitory molecule TIGIT selectively inhibit proinflammatory Th1 and Th17 cell responses. *Immunity.* 40:569–581. https://doi.org/10.1016/j.immuni.2014.02.012

Kerfoot, S.M., G. Yaari, J.R. Patel, K.L. Johnson, D.G. Gonzalez, S.H. Kleinstein, and A.M. Haberman. 2011. Germinal center B cell and T follicular helper cell development initiates in the interfollicular zone. *Immunity.* 34:947–960. https://doi.org/10.1016/j.immuni.2011.03.024

Kitano, M., S. Moriyama, Y. Ando, M. Hikida, Y. Mori, T. Kurosaki, and T. Okada. 2011. Bcl6 protein expression shapes pre-germinal center B cell dynamics and follicular helper T cell heterogeneity. *Immunity.* 34:961–972. https://doi.org/10.1016/j.immuni.2011.03.025

Kroenke, M.A., D. Eto, M. Locci, M. Cho, T. Davidson, E.K. Haddad, and S. Crotty. 2012. Bcl6 and Maf cooperate to instruct human follicular helper CD4 T cell differentiation. *J. Immunol.* 188:3734–3744. https://doi.org/10.4049/jimmunol.1103246

Laidlaw, B.J., Y. Lu, R.A. Amezquita, J.S. Weinstein, J.A. Vander Heiden, N.T. Gupta, S.H. Kleinstein, S.M. Kaech, and J. Craft. 2017. Interleukin-10 from CD4$^+$ follicular regulatory T cells promotes the germinal center response. *Sci. Immunol.* 2:eaan4767. https://doi.org/10.1126/sciimmunol.aan4767

Li, J., E. Lu, T. Yi, and J.G. Cyster. 2016. EBI2 augments Tfh cell fate by promoting interaction with IL-2-quenching dendritic cells. *Nature.* 533:110–114. https://doi.org/10.1038/nature17947

Lim, H.W., P. Hillsamer, and C.H. Kim. 2004. Regulatory T cells can migrate to follicles upon T cell activation and suppress GC-Th cells and GC-Th cell-driven B cell responses. *J. Clin. Invest.* 114:1640–1649. https://doi.org/10.1172/JCI200422325

Lim, H.W., P. Hillsamer, A.H. Banham, and C.H. Kim. 2005. Cutting edge: direct suppression of B cells by CD4+ CD25+ regulatory T cells. *J. Immunol.* 175:4180–4183. https://doi.org/10.4049/jimmunol.175.7.4180

Linterman, M.A., W. Pierson, S.K. Lee, A. Kallies, S. Kawamoto, T.F. Rayner, M. Srivastava, D.P. Divekar, L. Beaton, J.J. Hogan, et al. 2011. Foxp3+ follicular regulatory T cells control the germinal center response. *Nat. Med.* 17:975–982. https://doi.org/10.1038/nm.2425

Liu, Z., M.Y. Gerner, N. Van Panhuys, A.G. Levine, A.Y. Rudensky, and R.N. Germain. 2015. Immune homeostasis enforced by co-localized effector and regulatory T cells. *Nature.* 528:225–230. https://doi.org/10.1038/nature16169

Locci, M., C. Havenar-Daughton, E. Landais, J. Wu, M.A. Kroenke, C.L. Arlehamn, L.F. Su, R. Cubas, M.M. Davis, A. Sette, et al. International AIDS Vaccine Initiative Protocol C Principal Investigators. 2013. Human circulating PD-1+CXCR3-CXCR5+ memory Tfh cells are highly functional and correlate with broadly neutralizing HIV antibody responses. *Immunity.* 39:758–769. https://doi.org/10.1016/j.immuni.2013.08.031

Mandapathil, M., S. Lang, E. Gorelik, and T.L. Whiteside. 2009. Isolation of functional human regulatory T cells (Treg) from the peripheral blood based on the CD39 expression. *J. Immunol. Methods.* 346:55–63. https://doi.org/10.1016/j.jim.2009.05.004

Masopust, D., and J.M. Schenkel. 2013. The integration of T cell migration, differentiation and function. *Nat. Rev. Immunol.* 13:309–320. https://doi.org/10.1038/nri3442

McCarron, M.J., and J.C. Marie. 2014. TGF-β prevents T follicular helper cell accumulation and B cell autoreactivity. *J. Clin. Invest.* 124:4375–4386. https://doi.org/10.1172/JCI76179

Mempel, T.R., M.J. Pittet, K. Khazaie, W. Weninger, R. Weissleder, H. von Boehmer, and U.H. von Andrian. 2006. Regulatory T cells reversibly suppress cytotoxic T cell function independent of effector differentiation. *Immunity.* 25:129–141. https://doi.org/10.1016/j.immuni.2006.04.015

Miles, B., S.M. Miller, J.M. Folkvord, A. Kimball, M. Chamanian, A.L. Meditz, T. Arends, M.D. McCarter, D.N. Levy, E.G. Rakasz, et al. 2015. Follicular regulatory T cells impair follicular T helper cells in HIV and SIV infection. *Nat. Commun.* 6:8608. https://doi.org/10.1038/ncomms9608

Qi, H., J.L. Cannons, F. Klauschen, P.L. Schwartzberg, and R.N. Germain. 2008. SAP-controlled T-B cell interactions underlie germinal centre formation. *Nature.* 455:764–769. https://doi.org/10.1038/nature07345

Radtke, A.J., W. Kastenmüller, D.A. Espinosa, M.Y. Gerner, S.W. Tse, P. Sinnis, R.N. Germain, F.P. Zavala, and I.A. Cockburn. 2015. Lymph-node resident CD8α+ dendritic cells capture antigens from migratory malaria sporozoites and induce CD8+ T cell responses. *PLoS Pathog.* 11:e1004637. https://doi.org/10.1371/journal.ppat.1004637

Ritvo, P.G., G. Churlaud, V. Quiniou, L. Florez, F. Brimaud, G. Fourcade, E. Mariotti-Ferrandiz, and D. Klatzmann. 2017. T_{fr} cells lack IL-2Rα but express decoy IL-1R2 and IL-1Ra and suppress the IL-1-dependent activation of T_{fh} cells. *Sci. Immunol.* 2:eaan0368. https://doi.org/10.1126/sciimmunol.aan0368

Sage, P.T., and A.H. Sharpe. 2015. T follicular regulatory cells in the regulation of B cell responses. *Trends Immunol.* 36:410–418. https://doi.org/10.1016/j.it.2015.05.005

Sage, P.T., L.M. Francisco, C.V. Carman, and A.H. Sharpe. 2013. The receptor PD-1 controls follicular regulatory T cells in the lymph nodes and blood. *Nat. Immunol.* 14:152–161. https://doi.org/10.1038/ni.2496

Sage, P.T., A.M. Paterson, S.B. Lovitch, and A.H. Sharpe. 2014. The coinhibitory receptor CTLA-4 controls B cell responses by modulating T follicular helper, T follicular regulatory, and T regulatory cells. *Immunity.* 41:1026–1039. https://doi.org/10.1016/j.immuni.2014.12.005

Sage, P.T., N. Ron-Harel, V.R. Juneja, D.R. Sen, S. Maleri, W. Sungnak, V.K. Kuchroo, W.N. Haining, N. Chevrier, M. Haigis, and A.H. Sharpe. 2016. Suppression by T_{FR} cells leads to durable and selective inhibition of B cell effector function. *Nat. Immunol.* 17:1436–1446. https://doi.org/10.1038/ni.3578

Shulman, Z., A.D. Gitlin, S. Targ, M. Jankovic, G. Pasqual, M.C. Nussenzweig, and G.D. Victora. 2013. T follicular helper cell dynamics in germinal centers. *Science.* 341:673–677. https://doi.org/10.1126/science.1241680

Tran, D.Q., J. Andersson, R. Wang, H. Ramsey, D. Unutmaz, and E.M. Shevach. 2009. GARP (LRRC32) is essential for the surface expression of latent TGF-beta on platelets and activated FOXP3+ regulatory T cells. *Proc. Natl. Acad. Sci. USA.* 106:13445–13450. https://doi.org/10.1073/pnas.0901944106

Vaeth, M., G. Müller, D. Stauss, L. Dietz, S. Klein-Hessling, E. Serfling, M. Lipp, I. Berberich, and F. Berberich-Siebelt. 2014. Follicular regulatory T cells control humoral autoimmunity via NFAT2-regulated CXCR5 expression. *J. Exp. Med.* 211:545–561. https://doi.org/10.1084/jem.20130604

Wallin, E.F., E.C. Jolly, O. Suchánek, J.A. Bradley, M. Espéli, D.R. Jayne, M.A. Linterman, and K.G. Smith. 2014. Human T-follicular helper and T-follicular regulatory cell maintenance is independent of germinal centers. *Blood.* 124:2666–2674. https://doi.org/10.1182/blood-2014-07-585976

Wing, J.B., W. Ise, T. Kurosaki, and S. Sakaguchi. 2014. Regulatory T cells control antigen-specific expansion of Tfh cell number and humoral immune responses via the coreceptor CTLA-4. *Immunity.* 41:1013–1025. https://doi.org/10.1016/j.immuni.2014.12.006

Wing, J.B., Y. Kitagawa, M. Locci, H. Hume, C. Tay, T. Morita, Y. Kidani, K. Matsuda, T. Inoue, T. Kurosaki, et al. 2017. A distinct subpopulation of CD25$^-$ T-follicular regulatory cells localizes in the germinal centers. *Proc. Natl. Acad. Sci. USA.* 114:E6400–E6409. https://doi.org/10.1073/pnas.1705551114

Wollenberg, I., A. Agua-Doce, A. Hernández, C. Almeida, V.G. Oliveira, J. Faro, and L. Graca. 2011. Regulation of the germinal center reaction by Foxp3+ follicular regulatory T cells. *J. Immunol.* 187:4553–4560. https://doi.org/10.4049/jimmunol.1101328

Wu, H., Y. Chen, H. Liu, L.L. Xu, P. Teuscher, S. Wang, S. Lu, and A.L. Dent. 2016. Follicular regulatory T cells repress cytokine production by follicular helper T cells and optimize IgG responses in mice. *Eur. J. Immunol.* 46:1152–1161. https://doi.org/10.1002/eji.201546094

Ziegler, S.F., F. Ramsdell, and M.R. Alderson. 1994. The activation antigen CD69. *Stem Cells.* 12:456–465. https://doi.org/10.1002/stem.5530120502